Modelling of Transonic Buffet Alleviation via Spoilers

Andrea Petrocchi* and George N. Barakos†
CFD Laboratory, School of Engineering, University of Glasgow, Glasgow, G128QQ, Scotland, UK

In this work, computational fluid dynamics simulations are carried out to assess the ability of spoilers to alleviate transonic buffet. Spoilers are present on every commercial aircraft and can be used as shock and boundary-layer control devices. The difficulties to model slotted and deployable control surfaces have been overcome by adapting a formulation developped for modelling swinging Gurney flaps to wing spoilers. By adopting virtual spoilers, the separated region formed during buffet is divided. The shock is fixed to an upstream position, and the oscillations are stopped, or alleviated. The effectiveness of this buffet control method is first assessed using 2D computations around aerofoils with different sections and at different flow conditions. The sensitivity to the spoiler deployment angle is studied, and the optimum value based on the aerodynamic performance is determined. Then, computations on an OAT15A unswept wing are carried out to investigate the effect of the spoiler on the 3D buffet dynamics and flow topology.

Nomenclature

C_p	=	pressure coefficient $(p - p_\infty)/(0.5\rho U_\infty^2)$
C_D	=	drag coefficient $D/(0.5\rho U_\infty^2 c)$
C_L	=	lift coefficient $L/(0.5\rho U_\infty^2 c)$
C_μ	=	model constant
f_k	=	unresolved-to-total ratio of turbulent kinetic energy
f_ϵ	=	unresolved-to-total ratio of turbulent dissipation
f_ω	=	unresolved-to-total ratio of turbulent frequency
F_1, F_2	=	SST model blending functions
k	=	turbulent kinetic energy [m^2s^{-2}]
M_∞	=	Mach number
P_k	=	turbulent kinetic energy production term [$kg\,m^{-1}s^{-3}$]
$\mathbf{R}$	=	flow residual vector
Re_c	=	Reynolds number $\rho U_\infty c/\mu$
t	=	time [s]
U_i	=	flow velocity [ms^{-1}]
$V_{i,j,k}$	=	cell volume
x_i	=	spatial coordinates [m]
$\mathbf{W}$	=	flow variable vector
α	=	angle of attack [deg]
δ_s	=	spoiler deflection angle [deg]
$\dot{\delta_s}$	=	spoiler deflection rate [deg/s]
μ	=	molecular dynamic viscosity [$kg\,m^{-1}s^{-1}$]
μ_t	=	eddy viscosity [$kgm^{-1}s^{-1}$]
ν_t	=	kinematic eddy viscosity [m^2s^{-1}]
ω	=	turbulent frequency [s^{-1}]
ρ	=	density [$kg\,m^{-3}$]
β^*, β, γ, σ_k, σ_ω	=	SST model constants

*PhD Student, CFD Laboratory, James Watt School of Engineering, Email: Andrea.Petrocchi@glasgow.ac.uk.
†Professor, CFD Laboratory, James Watt School of Engineering, Email: George.Barakos@glasgow.ac.uk, MAIAA (Corresponding Author).

Acronyms

BILU	=	Block Incomplete Lower-Upper
CFD	=	Computational Fluid Dynamics
DDES	=	Delayed Detached-Eddy Simulations
DES	=	Detached-Eddy Simulations
GCG	=	Generalized Conjugate Gradient
GMRES	=	Generalized Minimum Residual
HMB	=	Helicopter Multi-Block
IDDES	=	Improved Delayed Detached-Eddy Simulations
LES	=	Large-Eddy Simulations
MUSCL	=	Monotone Upstream-centered Scheme for Conservation Laws
PANS	=	Partially Averaged Navier-Stokes
RANS	=	Reynolds-Averaged Navier-Stokes
SAS	=	Scale-Adaptive Simulations
SCB	=	Shock-Control Bumps
SIO	=	Shock-Induced Oscillation
SST	=	Shear Stress Tensor
TED	=	Trailing Edge Devices
URANS	=	Unsteady Reynolds-Averaged Navier-Stokes
VG	=	Vortex Generator

I. Introduction

Transonic buffet consists of self-sustained shock oscillations around aerofoils and wings. The phenomenon has been studied since the middle of the last century to shed light on the mechanism driving the shock oscillations. Buffet deteriorates the aircraft handling qualities and causes passenger discomfort in flight. Therefore, an airplane must be free from oscillations at any operating conditions and a buffet boundary is accounted for in the flight envelope to guarantee this requirement. Nonetheless, a variation of the flight conditions due to unexpected gusts or emergency maneuvers may cause the plane to cross the buffet boundary and undergo buffet. Therefore, attention has been paid to control ideas to eliminate or alleviate shock-induced oscillations (SIO).

A partial review of the flow control works for buffet is given in the work of Giannelis *et al.* [1]. The employed techniques distinguish mainly into vortex generators (VGs) [2–4], shock-control bumps (SCB) [5–8] and trailing edge devices (TED) [9–11]. All methods proved able to eliminate the shock oscillations at design conditions. Unfortunately, the first two categories of devices introduce installation drag, deteriorating the overall aerodynamic performance. This requires an expensive and sometimes unsuccessful work of optimization involving shape, number and position of the devices to minimize drag penalties. Such studies can be carried out for simple configurations [12, 13], but are overly expensive for full-wing geometries.

This paper presents an alternative to the aforementioned methods by taking advantage of surface controls present in every commercial airplane. According to the literature on buffet over 3D transonic wings, the buffet cells arise around 50-60% of the wingspan [14–16]. Spoilers can therefore be employed to alleviate buffet.

By deploying the control surface, the state of the boundary layer is altered and the buffet mechanism can be interrupted according to the most popular buffet mechanisms. The acoustic feedback mechanism of Lee [17] sees the downstream propagation of disturbances generated at the shock foot in the boundary layer. After reaching the trailing edge, they are scattered back and the pressure waves feed the shock motion. This mechanism was further investigated by several authors [18, 19] who confirmed the crucial role of upstream-travelling acoustic waves in feeding the shock motion. In the works from Crouch et al. [20, 21] and following works, e.g. [16, 22], transonic buffet was studied as a global flow instability. From their studies, buffet is seen as the result of a first unstable mode, involving the entire flow field. In both cases, the propagation of disturbances in the boundary layer is crucial. Whether one or the other explanation is preferred, the use of spoilers in hampering the mechanism seems reasonable. A sketch of the working principle compared to the mechanism of Lee [17] is given in fig. 1. Retracted in the wing, spoilers do not introduce installation drag nor off-design penalties like VGs or SCBs [23]. When buffet is detected, spoilers are deployed to reduce or suppress the SIO.

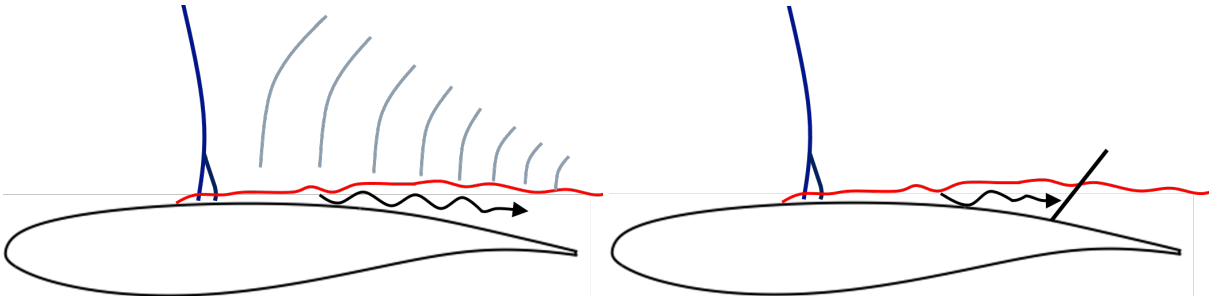

Fig. 1 Left: sketch of the acoustic feedback mechanism of Lee [17]; right: effect of the spoiler in stopping the downstream propagation of disturbances in the boundary-layer

The position within the wing and their mobility result in difficulties in modelling the spoilers. Therefore, the technique of Pastrikakis and Barakos [24] will be adopted to simulate virtual spoilers.

The paper is structured as follows: the mathematical model is presented in section II. There, attention is paid to the virtual spoiler modelling and the actuation strategy; section III is devoted to the flow control applications. The influence of the test section will be studied by comparing the results of 2D computations for the flow around two airfoils, the NACA0012 and the OAT15A. On the latter, a sensitivity study to the spoiler deflection angle was carried out. Among the pool of angles considered, the optimal value and a different, higher, one were tested on a 3D configuration with a finite wingspan to underline differences between the 2D and 3D cases; section IV is devoted to discussions and conclusions.

II. Numerical Method

A. Computational Model for Fluid Flow

Numerical simulations have been performed using the Helicopter Multi-Block (HMB3) [25, 26] flow solver, a three-dimensional, fully implicit, structured, code for the solution of the Navier-Stokes equations. The Navier-Stokes equations are discretized using a cell-centered finite volume approach. The computational domain is divided into a finite number of non-overlapping control volumes, and the governing equations are applied to each cell in turn. Also, the Navier-Stokes equations are re-written in a curvilinear co-ordinate system which simplifies the formulation of the discretized terms since body-conforming grids are adopted here. The spatial discretisation of the equations leads to a set of ordinary differential equations in time,

$$\frac{\mathrm{d}}{\mathrm{d}t}(\mathbf{W}_{ijk}V_{ijk}) = -\mathbf{R}_{ijk}(\mathbf{W}), \tag{1}$$

where $\mathbf{W}$ and $\mathbf{R}$ are the vectors of cell conserved variables and residuals respectively, and V is the cell volume. The convective terms are discretized using Osher's upwind scheme [27]. A monotone upstream-centered scheme for conservation laws (MUSCL) variable extrapolation [28] is used to provide second-order accuracy with the Van Albada limiter [29] to prevent spurious oscillations around shock waves. For the integration in time, the implicit dual-time stepping method of Jameson [30] is used.

The linearized system of equations is solved using the generalized conjugate gradient (GCG) method with a block incomplete lower–upper (BILU) factorization as a pre-conditioner [31]. The Jacobian is approximated by evaluating the derivatives of the residuals with a first-order scheme for the inviscid fluxes. The first-order Jacobian requires less storage and ensures a better convergence rate to the GCG iterations. The steady-state solver for turbulent flows is formulated and solved in an identical manner to that of the mean flow. The eddy-viscosity is calculated from the latest values of the turbulent variables, e.g. k and ω, and is used to advance the mean and the turbulent flow solutions. An approximate Jacobian is used for the source term of the models by only taking into account the contribution of their dissipation terms, i.e. no account of the production terms is taken on the left-hand side of the system. The solver offers several one-, two-, three-, and four-equation turbulence models. In addition, LES, DES, delayed DES (DDES), improved DDES (IDDES), SAS and PANS methods are available.

B. PANS formulation

The partially-averaged Navier-Stokes (PANS) formulation [32] is a bridging model between RANS and DNS. The formulation is based on a RANS paradigm, where the blending is obtained by means of the user-prescribed unresolved-to-total ratios of turbulent kinetic energy f_k and dissipation f_ϵ, bounded between 0 and 1, acting on the turbulence closure equations. They read: $f_k = k_u/k$, $f_\epsilon = \epsilon_u/\epsilon$, where the u subscripts stands for unresolved and the quantities at the denominator are the total ones. The PANS method was initially derived for k-ϵ closures and then extended to the Wilcox k-ω model [33] by Lakshmipathy et al. [34] and to the Menter SST model [35] by Luo et al. [36]. In k-ω based formulations the parameter f_ϵ is replaced by the unresolved-to-total turbulence frequency $f_\omega = \omega_u/\omega = f_\epsilon/f_k$. These formulations inherit from the parent RANS models an eddy viscosity based on a Boussinesq approximation, that is reduced with respect to the RANS case because of the effects of the f_k parameter; since only a fraction of the turbulent kinetic energy is modelled, the corresponding value of the eddy viscosity is reduced. This gives the possibility for the turbulent structures to be resolved. When adopting a reasonably high value of f_k the method can be used as a less dissipative version of URANS.

In this work the SST-PANS formulation is adopted. It reads:

$$\frac{\partial(\rho k)}{\partial t} + \frac{\partial(\rho U_j k)}{\partial x_j} = P_k - \beta^* \rho k \omega + \frac{\partial}{\partial x_j}\left[\left(\mu + \mu_t \sigma_k \frac{f_\omega}{f_k}\right)\frac{\partial k}{\partial x_j}\right], \tag{2}$$

$$\frac{\partial(\rho\omega)}{\partial t} + \frac{\partial(\rho U_j \omega)}{\partial x_j} = \frac{\gamma}{\nu_t} P_k - \beta' \rho \omega^2 + \frac{\partial}{\partial x_j}\left[\left(\mu + \mu_t \sigma_\omega \frac{f_\omega}{f_k}\right)\frac{\partial \omega}{\partial x_j}\right] + 2\frac{f_\omega}{f_k}(1 - F_1)\frac{\rho\sigma_{\omega 2}}{\omega}\frac{\partial k}{\partial x_j}\frac{\partial \omega}{\partial x_j}, \tag{3}$$

where ρ is the density, U_j is the flow velocity, μ is the dynamic molecular viscosity and μ_t is the turbulent viscosity. Here, the turbulent kinetic energy k and frequency ω are the modelled, or unresolved, fraction where the subscripts were dropped for sake of simplicity. In the ω-equation, $\beta' = \left(\gamma\beta^* - \frac{\gamma\beta^*}{f_\omega} + \frac{\beta}{f_\omega}\right)$; F_1 is the blending function while $\gamma, \beta, \beta*, \sigma_k, \sigma_\omega$ are the model constants, calculated as prescribed in reference [35]. The eddy viscosity has the same form as in the formulation of the SST model.

C. Spoiler Modelling

The spoiler is modelled following the implementation in HMB3 of Pastrikakis and Barakos [24, 37] for Gurney flaps. In fig. 2, right image, the mesh adopted around the OAT15A with spoilers is shown. To build such a grid around the spoiler location, a hinge (see. fig. 2, left image) must be introduced. Using this grid topology, the virtual spoiler can

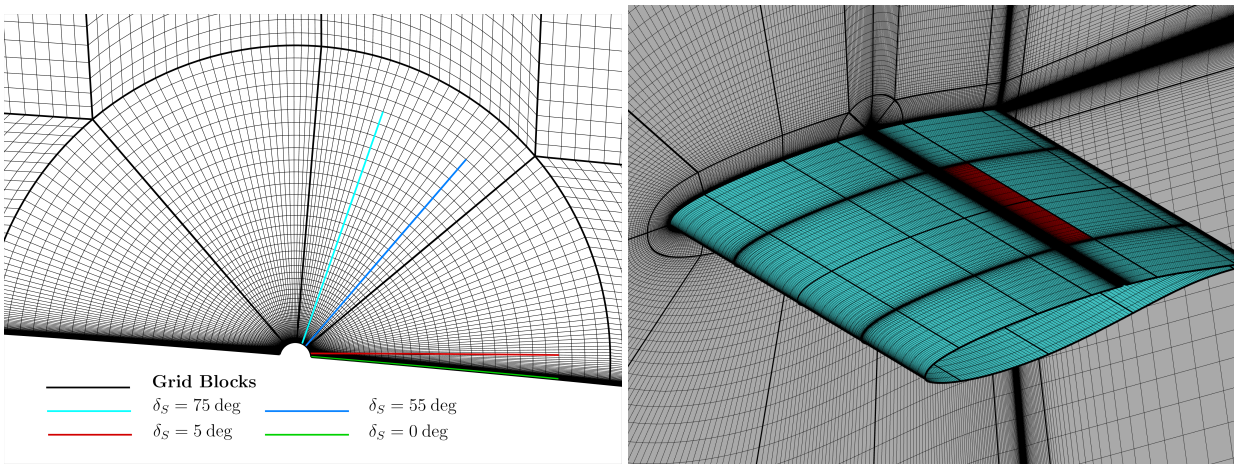

Fig. 2 Left: airfoil sketch with hinge (red); right: mesh around the 3D OAT15A wing section, with spoiler.

be simulated by flagging cell faces corresponding to its position as boundary faces and imposing no-slip boundary conditions. Adopting this method, once the grid is properly built, no additional effort is required in terms of mesh generation, and the moving surface can be modelled without the need for overset method or overly fine grids. Fig. 2 shows a close view of the hinge location with the spoiler deployed at different angles. No-slip boundary conditions are

imposed on the coloured cell faces. Given the multi-block nature of the solver, the user can specify within which blocks the spoiler is contained. In this case, only the first two rightmost blocks around the hinge are flagged as *spoiler blocks*. Therefore, the spoiler cannot be deployed more than, roughly, 90 degrees from its initial position. The spoiler position is given in input by specifying three points corresponding to the beginning and end of the hinge and a third point to define the spoiler plane. Once the initial spoiler position is calculated, it can be deployed by following a linear law or a arbitrary law based on a summation of harmonics.

To determine the instantaneous spoiler position and the corresponding boundary flags, the algorithm used in this work is the same used in [37] and repeated in algorithm 1.

Algorithm 1 Pseudo-code for spoiler definition.

```
Find the spoiler size
Find the spoiler angle
for all spoiler blocks in the mesh do
    if the point is inside the radius then
        Flag the cells behind and in front of the spoiler with -1 and 1
    else
        Flag the cells behind and in front of the spoiler with -2 and 2
    end if
end for
Sweep along the lines
if the sign changes between two cells then
    if the sum of the four neighbor cells of a node is 6 then
        This node is the end of the spoiler
    end if
end if
All the cell faces up to that node will be flagged as boundary cells
```

1. Active Control

Buffet control by means of spoilers could be made automatic by using probes in the boundary layer to detect separation. At design conditions, local flow separation can occur at the shock foot, while in buffet regimes the separated flow region extends, during a fraction of the buffet period, from the shock foot to the leading edge. In this view, the idea is to place a sensor in the boundary layer at a strategic location, i.e. where separation is not expected, and exploit the information at that point to activate flow control when required.

The sketch of fig. 3 illustrates the control point for buffet detection. The probe is located on the airfoil surface at $x/c = 0.7$ and samples the conserved flow variables at each timestep. The probe is at a distance $\Delta y/2$ from the wall, being Δy the normal spacing of the first cell. When flow reversal is detected the spoiler is deployed following a linear law:

$$\delta = \delta_0 + \min(\dot{\delta}(t - t_{B,0}), \delta_{\max}) \,, \tag{4}$$

where δ_0 is the position of the undeployed spoiler, $\dot{\delta}$ is the user-described angular velocity, assumed constant over the spoiler excursion, and $\delta_{\max}$ is the maximum displacement. We indicated with $t_{B,0}$ the instance when buffet is first detected. This is implemented by applying a discrete increment for each timestep:

$$\delta^i = \delta_0 + \min(\dot{\delta}(t_i - t_{B,0}), \delta_{\max}) \,, \quad \dot{\delta} = \delta_{\max} \Delta t_{act} \,, \quad \Delta t_{act} = 1/N_{act} \,, \tag{5}$$

where the velocity is specified by means of the parameter Δt_{act}, equal to the inverse of the number of unsteady steps required to deploy the device N_{act}.

III. Results and Discussion

In this section, the effect of infinite and finite virtual spoilers will be investigated. In a previous publication [38], the accuracy of the PANS model to cope with the two configurations under analysis (the OAT15A and the NACA0012) at buffet conditions was established. The PANS model based on a k $-$ ω SST model gave good results for the 2D case and

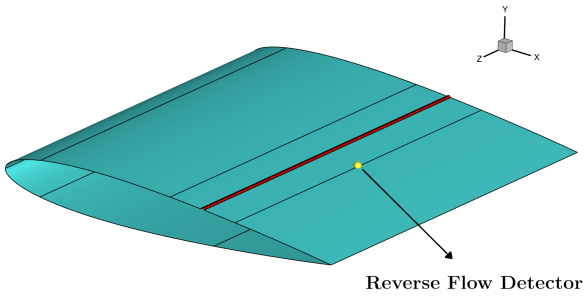

Fig. 3 Sketch of the buffet sensor employed around a NACA0012 airfoil.

will be employed for the remainder of this work. Results for the infinite spoiler, i.e. for 2D computations, were presented using both static and active control. Some aspects related to the influence of the wing section on the aerodynamic performance are discussed. 3D computations with finite spoilers are presented and compared with the 2D cases.

A. Test Case Description

1. OAT15A Wing Section

The supercritical OAT15A wing section was analyzed in the S3Ch wind tunnel at ONERA [39, 40]. The wing section has a chord of $c = 0.23$m and a span, coinciding with that of the tunnel, of 0.78 m. The section has a thickness-to-chord ratio of $t/c = 0.123$ and a trailing edge thickness of 0.5% of the chord. The wing was mounted in a squared section wind tunnel having nominal dimensions of $0.78\text{m} \times 0.78\text{m} \times 2.2\text{m}$. An adaptation technique based on a steady flow hypothesis was used at the lower and upper walls to reproduce free-stream conditions. Measurements were collected at free-stream Mach numbers in the range of 0.7-0.75, a chord-based Reynolds number of $\text{Re}_c = 3 \times 10^6$ and angle of attack in the range of 1.36 - 3.9 deg. The adoption of static pressure measurements and Kulite sensors distributed in the vicinity of the mid-span section allowed to detect the occurrence of flow unsteadiness at an angle of attack of 3.1 deg at $\text{M}_\infty = 0.73$ and 3.5 deg at $\text{M}_\infty = 0.72$. For the case at $\text{M}_\infty = 0.73$ and $\alpha = 3.5$ deg, a laser Doppler velocimetry (LDV) system was used to acquire velocity-field data and compute statistics. Although a large characterization of the buffet onset was provided, the available data was used to assess the exactness of the time-marching simulation for the documented buffet flow.

In this work, simulations at $\text{Re}_c = 3 \times 10^6$, $\text{M}_\infty = 0.73$ and $\alpha = 3.5$ ($\simeq 0.4$ deg above the onset) deg were carried out.

NACA0012 Wing Section

The second test section analyzed, the NACA0012 section, was studied at the Ames High Reynolds Number Facility by McDevitt and Okuno [41]. Mach numbers are in the range of 0.71-0.8 and Reynolds number span between 1 and 10 million. The buffet onset was detected by means of steady and unsteady pressure measurements. The tunnel walls were adapted to follow the free air streamlines, while the sidewall interference was reduced by thinning the sidewall boundary layer by means of suction applied on porous panels. Further details are given in the reference. Although these experiments are more than 30 years old, they still represent the broadest database for buffet onset, covering a wide range of conditions. Moreover, the treatment of the wind tunnel wall allowed to consider the flow as close as possible to a perfectly 2D flow, making this test case particularly suitable for this study.

Here, simulations at $\text{Re}_c = 10 \times 10^6$, $\text{M}_\infty = 0.72$ and $\alpha = 6.0$ ($\simeq 2.0$ deg above the onset) deg were carried out.

B. Grid and Numerical Setup

The unsteady computations were carried out using a PANS approach with the SST model as a RANS parent. The PANS formulation was detailed in sec. II.B. The adoption of PANS allowed for the unlocking of the flow oscillations. Adopting reasonably high values of the parameter f_k ($f_k = 0.7$ here), a PANS formulation can help in the prediction of this class of flows, where most statistical turbulence models give too high levels of eddy viscosity [42, 43], even working in RANS mode and for 2D simulations. Very good agreement was found between PANS and experiments for

the aforementioned configurations. On the other hand, URANS simulations with the SST model led to a steady-state solution even at angles of attack well beyond the buffet onset. The failure of the SST model to accurately predict buffet was also observed in other published works [42, 43].

The computational grids used for the aerofoils have a typical C-H topology. The 2D grid consists of $N_{\text{airfoil}} = 756$ cells around the aerofoil, of which $N_{\text{hinge}} = 228$ for the hinge and $N_{TE} = 60$ for the trailing edge (for blunt TE), $N_y = 170$ cells in the normal direction, and $N_w = 110$ cells in the wake, for a total of about 120 thousand cells over the domain extending $80c$ both ahead of the aerofoil, and in the wake direction. The spacing distribution has been set to satisfy the condition of $\Delta y^+ < 1$ at each condition, resulting in a first cell size of about $2.0 - 5.0 \times 10^{-6} c$ for the aforementioned flow conditions. Adiabatic wall conditions were imposed at the aerofoil, and free-stream values of pressure and velocity elsewhere. For the time-marching computations, a timestep of $\Delta t = 0.01 c/U_\infty$ was employed, and corresponds to 1500 and 1200 unsteady steps for the OAT15A and NACA0012 sections, respectively. The convergence of the implicit scheme was based on the reduction of the flow field residual with respect to the previous step. In particular, either 3 orders of magnitude of reduction or 100 inner iterations of the dual-time stepping scheme were reached for each unsteady step.

The CFD domain for the 3D computations has an extension of $L_z = c$ in the span and is discretized using $N_z = 100$ cells in the spanwise direction. A refinement around the two spoiler ends was applied to allow for an adequate resolution of the longitudinal vortices expected in that region. The final grid consists of around 14 million points. In this case, periodic boundary conditions were applied at the sidewalls. Fig. 2, right image, shows the grid employed for the 3D computation, where the 2D grid in the grey plane is the same adopted for the 2D calculations. The hinge, covering the whole span, is placed at $0.6c$ from the aerofoil leading edge, has a radius of $r_h = 0.00625c$, and extends for half the span.

C. 2D Control case

Here are the results in the case of static control.

1. NACA0012 simulations

At buffet conditions around the NACA0012 airfoil, the spoiler deployment angles amounted to 10 and 20 deg. When the spoiler is not deployed, $\delta = 0$ deg in fig. 4, the only presence of the hinge slightly dampens the oscillations and this is reflected in the lift coefficient history in fig. 4. When the spoiler is deployed the oscillations are suppressed, with a transient time that shortens as δ_s increases. Fig. 5 shows the effect of the spoiler on the separated region. In

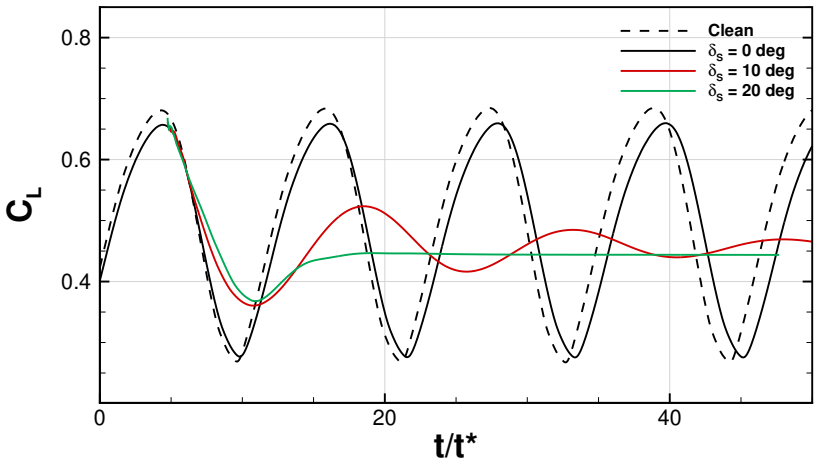

Fig. 4 Aerodynamic coefficients history for different angles of spoiler deployment δ on the NACA0012 at $\mathbf{Re}_c = 10 \times 10^6$, $\mathbf{M}_\infty = 0.72$ and $\alpha = 6.0$ deg.

this case, the separation region is perturbed in the first case and broken into two parts in the second case. This results in a stabilization of the shock position. This case is a particular one because the separation is prominent even for the baseline flow. Therefore, once the spoiler is added, the size of the separated region does not vary significantly and the spoiler only contributed by avoiding the propagation of disturbances in the boundary layer. For smaller δ_s, the separated flow region is not completely broken and, therefore, the transient is longer. For this case, the values of the aerodynamic

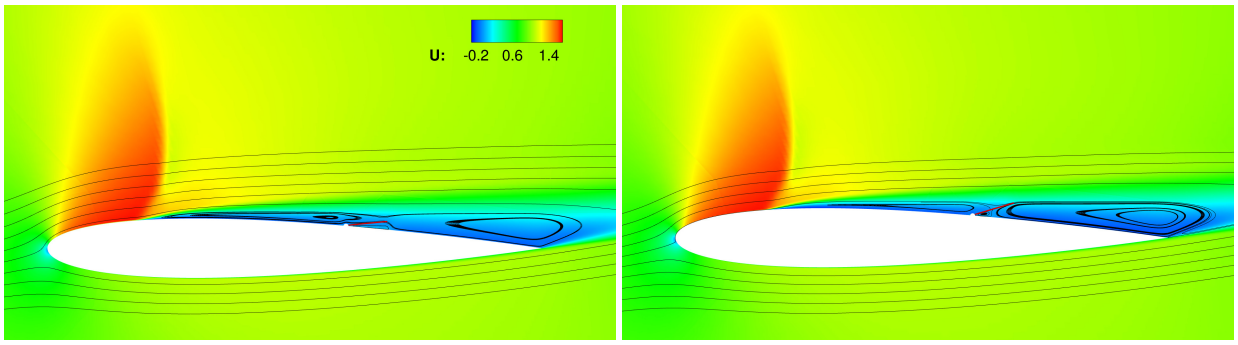

(a) δ_S = 5 deg (b) δ_S = 15 deg

Fig. 5 Steady-state, streamwise velocity contour with streamlines for different angles of spoiler deployment δ on the NACA0012 at $Re_c = 10 \times 10^6$, $M_\infty = 0.72$ and $\alpha = 6.0$ deg. The spoiler is indicated in red.

coefficients at steady-state did not differ significantly from the average one in the baseline case.

2. OAT15A simulations

For the OAT15A case, the history of the aerodynamic coefficients in response to an instantaneous deployment of the spoiler at different angles δ_s is shown in fig. 6. In table 1, the contribution given by the spoiler is distinguished from the part of the loads that does not account for the additional surface. Also, the viscous and pressure contributions on the drag are distinguished. The values at steady-state of the four coefficients are collected in table 1.

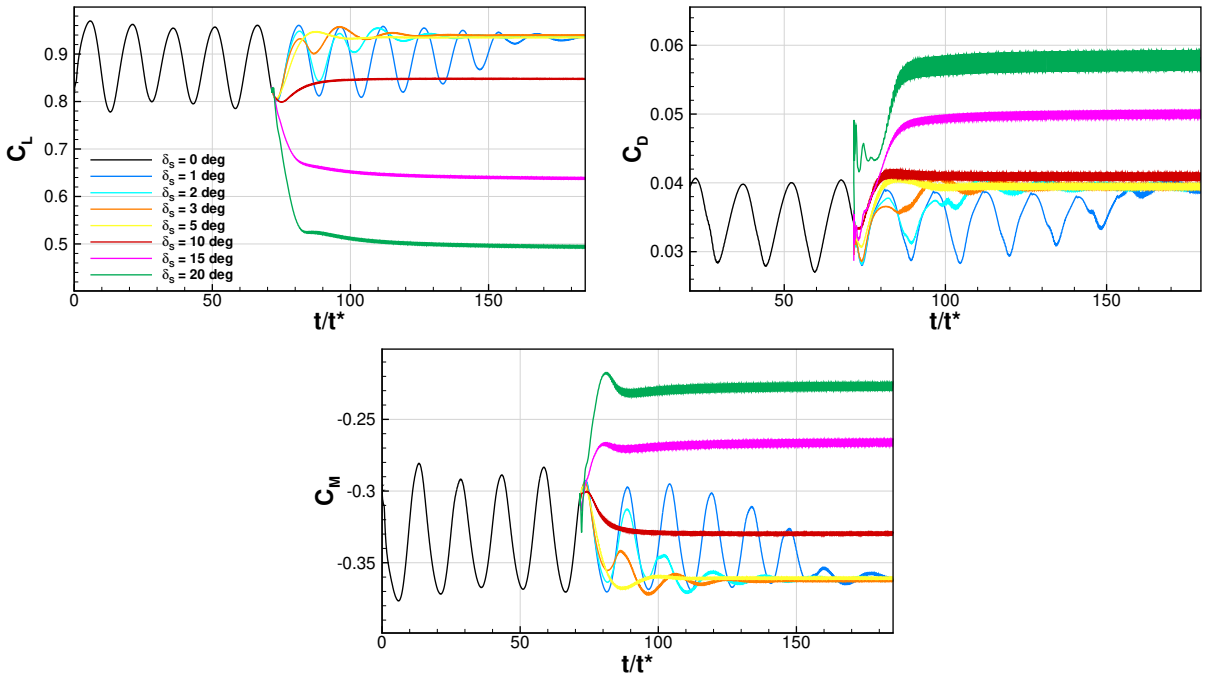

Fig. 6 Aerodynamic coefficients history for different angles of spoiler deployment δ on the OAT15A aerofoil at $Re_c = 3 \times 10^6$, $M_\infty = 0.73$ and $\alpha = 3.5$ deg.

The lift coefficient (fig. 6, top left) tends towards a steady state value even for a small deflection of the spoiler. Unlike the NACA0012 case, a small deflection of the spoiler cancels buffet. The lift increase is not due to the presence of the spoiler itself but to the ability of the device to stabilize the shock at a position that is downstream of the mean position

during the buffet motion. A drawback is the increase in drag with respect to the uncontrolled case (fig. 6, top right). In the previous case of prominent separation, the spoiler was immersed in the separation flow region and no significant pressure difference arose between the two faces. Therefore, such a significant drag penalty was not found. This can be further appreciated in fig. 7, where a net pressure jump at the hinge location is visible for all the values of δ_s. The pressure jump has a local minimum for $\delta_s = 5$ deg, and increases significantly at higher angles, where the spoiler no longer represents a shock control device and behaves as an air-breaker. The pitching moment (fig. 6, bottom) increases, since the separation region created behind the spoiler results in a local separation that modifies the load distribution.

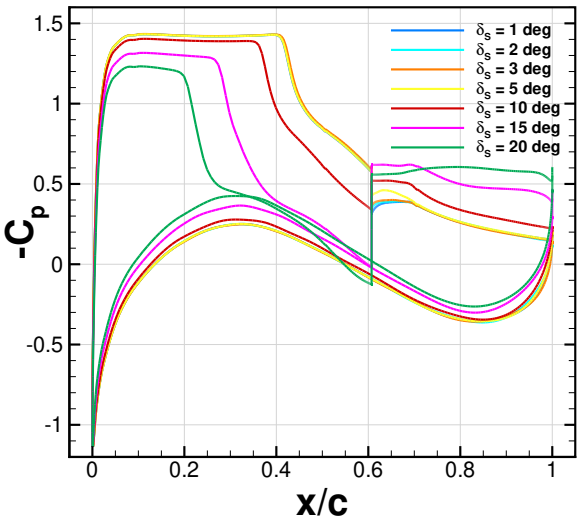

Fig. 7 Pressure coefficient distribution for different angles of spoiler deployment δ around the OAT15A aerofoil, $\mathbf{Re}_c = 3 \times 10^6$, $\mathbf{M}_\infty = 0.73$ and $\alpha = 3.5$ deg.

Table 1 Steady-state aerodynamic coefficient for different spoiler deflection angles for the OAT15A aerofoil, $\mathbf{Re}_c = 3 \times 10^6$, $\mathbf{M}_\infty = 0.73$ and $\alpha = 3.5$ deg.

δ_s [deg]	$\overline{C_L}$	$\overline{C_{L_s}}$	$\overline{C_{D,p}}$	$\overline{C_{D,p_s}}$	$\overline{C_{D,v}}$	$\overline{C_{D,v_s}}$	$\overline{C_m}$	$\overline{C_{m_s}}$	t_{ss}/t^*
0	0.867		0.0346		0.00375		-0.327		
1	0.927	0.0085	0.0398	0.0011	0.00411	0.00035	-0.359	-0.00061	$\simeq 150$
2	0.929	0.0079	0.0392	0.0009	0.00399	0.00022	-0.361	-0.00058	$\simeq 90$
3	0.933	0.0072	0.0396	0.0007	0.00392	0.00015	-0.363	-0.00053	$\simeq 85$
5	0.927	0.0019	0.0396	0.0001	0.00379	0.00005	-0.362	-0.00036	$\simeq 50$
10	0.838	-0.0146	0.0404	0.0004	0.00346	-0.00006	-0.331	0.00016	$\simeq 45$
15	0.625	-0.0374	0.0494	0.0045	0.00353	-0.00009	-0.265	0.00094	$\simeq 110$
20	0.485	-0.0416	0.0570	0.0082	0.00368	-0.00006	-0.224	0.00134	$\simeq 110$

To better understand the effect the spoiler has at different locations, longitudinal velocity contours are shown in fig. 8 for a spoiler deflection angle of $\delta_s = 5$, 10, 20. The separated flow region behind the spoiler acts by reducing the angle of attack and pushing the shock close to the leading edge where it loses strength. This effect is more evident as δ_s increases. For $\delta_s = 5$ deg, the shock is strong enough to separate the boundary layer and the spoiler breaks the communication between the two recirculation regions. In the other two cases, the shock is pushed further upstream and the boundary layer is attached upstream of the spoiler.

D. 3D Control

Here the results for the finite spoiler case applied on the OAT15A wing are presented. The investigated angles of attack are $\delta_s = 5$, 15 deg. The first is optimum for the 2D case when it comes to lift increase and time of actuation, while the second is an off-design actuation.

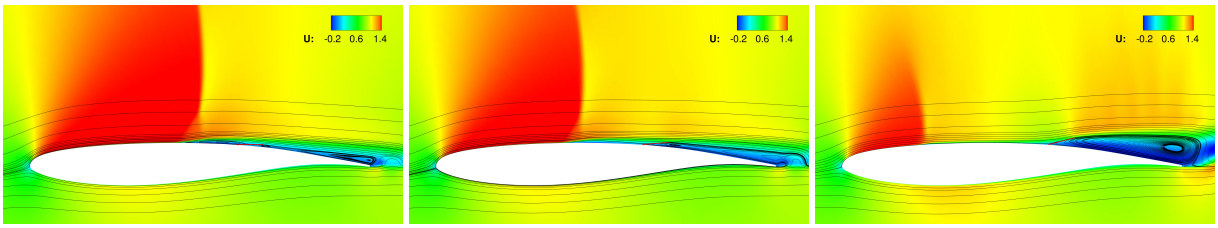

(a) $\delta_S = 5$ deg (b) $\delta_S = 10$ deg (c) $\delta_S = 20$ deg

Fig. 8 Streamwise velocity component contours for different angles of spoiler deployment δ_s on the OAT15A aerofoil at $\mathbf{Re}_c = 3 \times 10^6$, $\mathbf{M}_\infty = 0.73$ and $\alpha = 3.5$ deg. The spoiler is indicated in red.

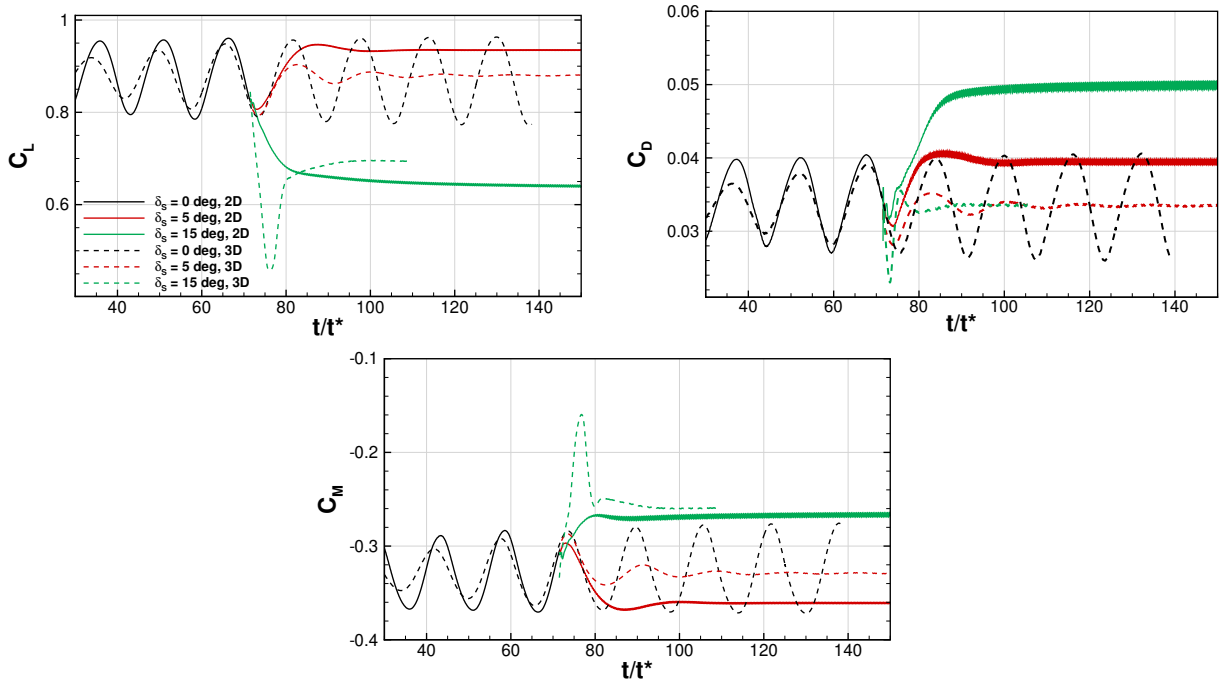

Fig. 9 Aerodynamic coefficients history for 2D and 3D simulations on the OAT15A wing section at $\mathbf{Re}_c = 3 \times 10^6$, $\mathbf{M}_\infty = 0.73$ and $\alpha = 3.5$ deg.

Figure 9 shows the influence of flow control on the aerodynamic coefficients. In every case, the SIO is suppressed within some buffet period. With respect to the 2D counterpart, the 3D case at $\delta_s = 5$ deg is affected by the limited spanwise extent of the flow control device and the response time is increased. The same holds for the effect that the spoiler has on the steady-state value of the aerodynamic coefficient. This is extremely positive when one looks at the drag coefficient, that drop significantly with respect to the 2D case. The steady-state values of the aerodynamic coefficients, for the case $\delta_s = 5$, now roughly coincide with their mean value at buffet conditions. The delay in the time response is not significant: given the frequency of buffet, a response time of $3 \div 5$ buffet periods corresponds to less then 0.1 s, which is more than satisfactory for every practical application. The situation is similar for the $\delta_s = 15$ case.

The steady-state pressure distribution in fig. 10, shows, at both angles, a curved shock front. The shock, in agreement with the 2D cases, is pushed upstream. This effect is more significant at the spanwise positions corresponding to the presence of the spoiler. This reflects in a shock position that is more downstream with respect to the 2D case. In the $\delta_s = 15$ case, the flow is compressed between the shock and the spoiler, accentuating the pressure jump across the hinge. The high δ_s case sees a stronger 3D effect.

Friction lines in fig. 11 complement the results of fig. 10 and corroborate those of the 2D computations. The $\mathrm{M}_\infty = 1$ iso-surfaces show the shock position, the $U/U_0 = -0.001$ iso-surfaces indicate the extent of the separated regions, and

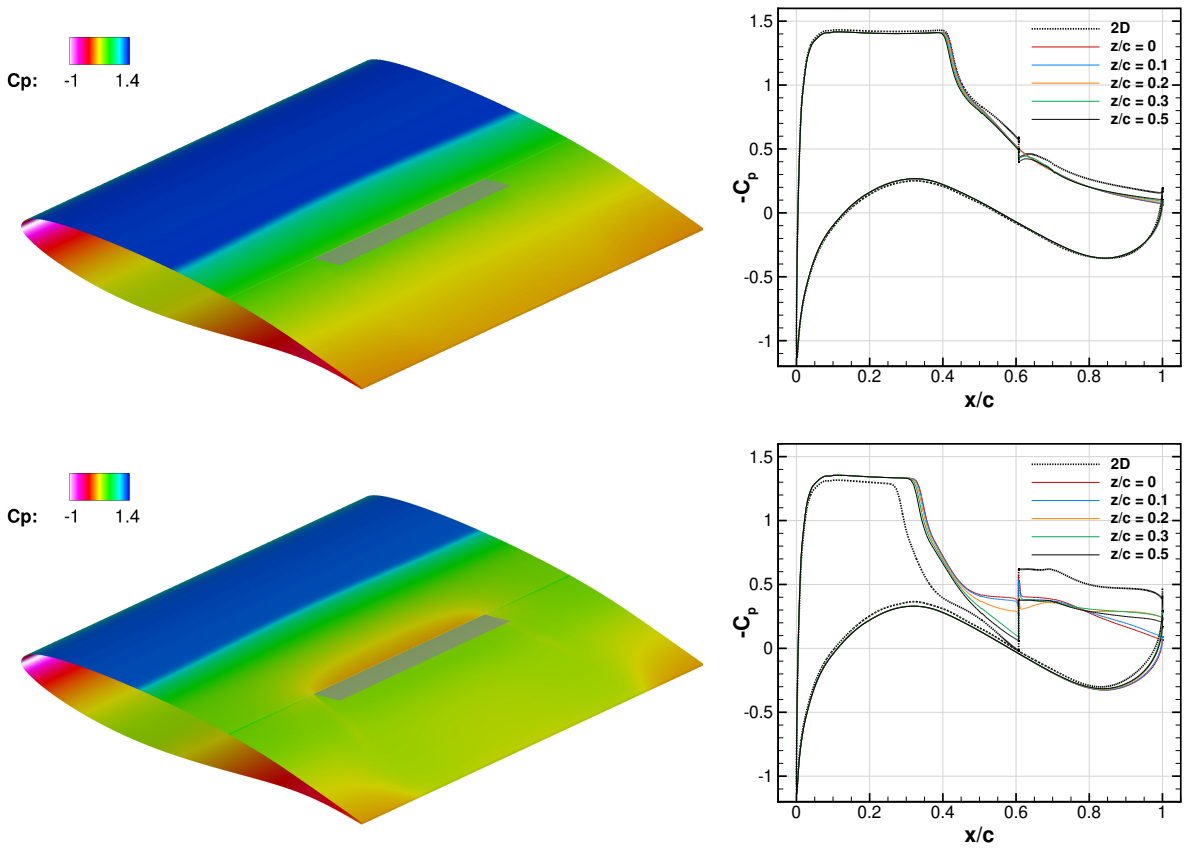

Fig. 10 Isocontour (left) and line plots at different spanwise locations (right) of the pressure coefficient around the OAT15A wing at $Re_c = 3\times10^6$, $M_\infty = 0.73$ and $\alpha = 3.5$ deg. $z/c = 0$ corresponds to the domain sidewall while $z/c = 0.5$ corresponds to the symmetry plane. Dashed, black lines indicate the results of the 2D computations at the same angles. Top: $\delta_s = 5$ deg; bottom: $\delta_s = 15$ deg.

the friction lines help to visualize the spanwise flow organization. In the $\delta_s = 5$ case, the rear shock position results in a separated flow region spanning from the shock foot to the spoiler, while for a higher spoiler angle, an aft shock position allows the boundary layer to re-attach. In the latter, the flow decelerates before turning around the spoiler, as it happens air-breakers, resulting in a higher pressure jump across the control surface and drag penalty. The results are in line with the 2D cases. The main difference consists of the flow structure out of the portion covered by the spoiler, where the flow re-attaches. Therefore, the effect of the finite control surface is mitigated.

The pressure difference between the upper and lower surface of the spoiler results in two counter-rotating tip vortices which are well captured in the computations. The higher the δ_s, the more intense the vortices, as shown in fig. 12.

IV. Conclusions and Future Work

In this work, numerical simulations of spoilers on wing sections are used to alleviate the shock-induced oscillations associated with transonic buffet. A PANS model based on a k-ω SST model was used for simulations of the flow around two- and three-dimensional configurations and provided accurate results for the prediction of the SIO.

The presence of the surface proved able in hampering the communication between the shock-foot and the trailing edge separation regions. Two airfoils were investigated in the 2D campaign: the NACA0012 and the OAT15A aerofoils. In the first case, because of the flow conditions and the airfoil geometry, the separated flow region in the buffet case was much larger. Therefore, a greater spoiler deployment was necessary to suppress buffet. In the second case, even a small angle deployment of the spoiler was revealed effective in reducing the SIO. On the second configuration, 3D simulations were repeated adopting a finite spoiler at two deployment angles. The limited span of the control surface resulted in a

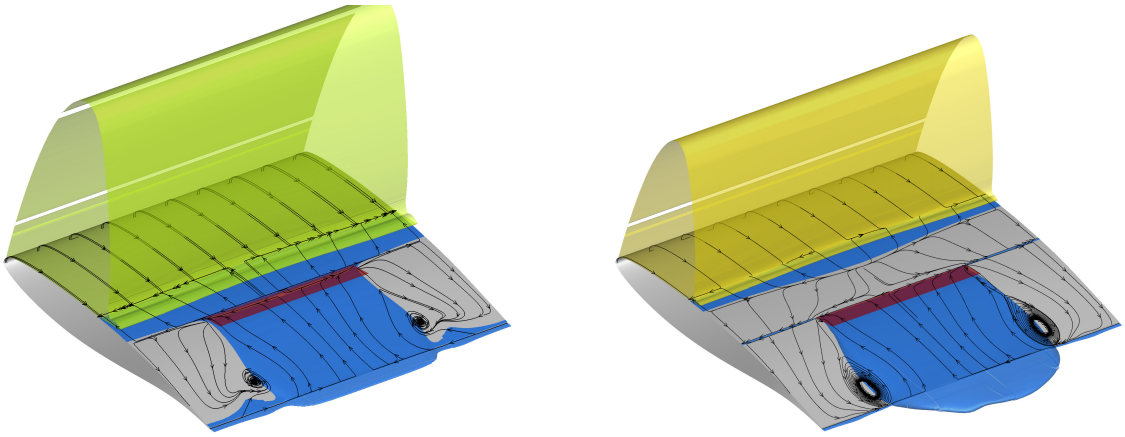

(a) $\delta_S = 5$ deg (b) $\delta_S = 15$ deg

Fig. 11 $\mathbf{M}_\infty = 1$ (yellow) and $U/U_0 = -0.001$ (blue) iso-surfaces for the flow around the OAT15A wing at $\mathbf{Re}_c = 3 \times 10^6$, $\mathbf{M}_\infty = 0.73$ and $\alpha = 3.5$ deg. The spoiler is indicated by the red surface.

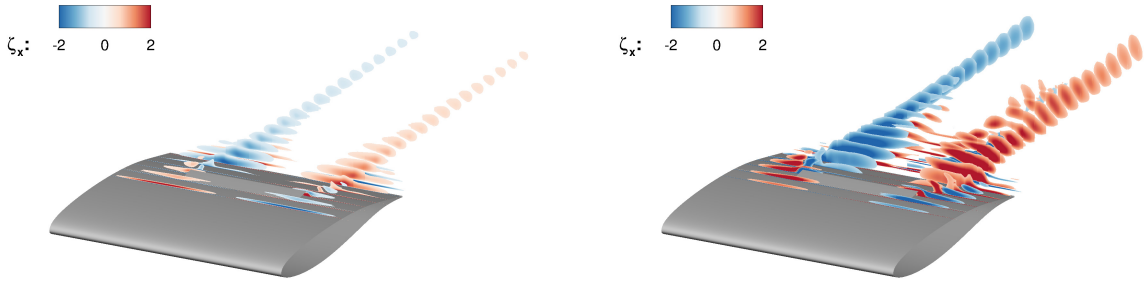

(a) $\delta_S = 5$ deg (b) $\delta_S = 15$ deg

Fig. 12 Longitudinal component of the vorticity vector around the OAT15A wing at $\mathbf{Re}_c = 3 \times 10^6$, $\mathbf{M}_\infty = 0.73$ and $\alpha = 3.5$ deg.

mitigation of its effect compared to the 2D case. At a higher deployment angle, the separation behind the spoiler is more severe, and the device acts as an air-breaker. Overall, the work showed the ability to reproduce the effect of spoilers by using a virtual control surface, and two test cases suggest that spoilers were effective in suppressing buffet.

The results showed a dependency on the wing section geometry and the angle of deployment of the spoiler. Future studies will be devoted to the sensitivity of the performance to the spoiler position, extent and strategy of actuation.

Acknowledgments

The present work is supported by the TEAMAero European project No. 860909 - Towards Effective Flow Control and Mitigation of Shock Effects In Aeronautical Applications. The use of the Cirrus system of EPCC for HPC is gratefully acknowledged.

Bibliography

[1] Giannelis, N., Vio, G., and Levinski, O., "A review of recent developments in the understanding of transonic shock buffet," *Progress in Aerospace Sciences*, Vol. 92, 2017, pp. 39–84. http://doi.org/10.1016/j.paerosci.2017.05.004.

[2] Molton, P., Dandois, J., Lepage, A., Brunet, V., and Bur, R., "Control of buffet phenomenon on a transonic swept wing," *AIAA*

Journal, Vol. 51, 2013, pp. 761–772. http://doi.org/10.2514/1.J051000.

[3] Dandois, J., Lepage, A., Dor, J.-B., Molton, P., Ternoy, F., Geeraert, A., Brunet, V., and Coustols, E., "Experimental study of transonic buffet phenomenon on a 3D swept wing," *Comptes Rendus Mécanique*, Vol. 342, 2014, pp. 425–436. http://doi.org/10.1016/j.crme.2014.01.015.

[4] Masini, L., Peace, A., and Timme, S., "Influence of Vane Vortex Generators on Transonic Wing Buffet: Further Analysis of the BUCOLIC Experimental Dataset," *52nd 3AF International Conference on Applied Aerodynamics*, Lyon, France, 2017.

[5] Birkenmeyer, J., Rosemann, H., and Stanewsky, E., "Shock control on a swept wing," *Aerospace Science and Technology*, Vol. 4, 2000, pp. 147–156. https://doi.org/10.1016/S1270-9638(00)00128-0.

[6] Mayer, R., Lutz, T., and Kramer, E., "Numerical Study on the Ability of Shock Control Bumps for Buffet Control ," *AIAA Journal*, Vol. 56, 2018, pp. 1978–1987. http://doi.org/10.2514/1.J056737.

[7] Mayer, R., Lutz, T., and Kramer, E., "Control of Transonic Buffet by Shock Control Bumps on Wing-Body Configuration," *AIAA Journal*, Vol. 56, 2019, pp. 556–568. http://doi.org/10.2514/1.C034969.

[8] D'Aguanno, A., Schrijer, F., and van Oudheusden, B., "Investigation of 3D Shock Control Bumps for Transonic Buffet Alleviation," *AIAA Aviation 2021 Forum*, Virtual Event, 2021.

[9] Caruana, D., Mignosi, A., Robitaillié, C., and Corrège, M., "Separated Flow and Buffeting Control," *Flow, Turbulence and Combustion*, Vol. 71, 2003, pp. 221–245. http://doi.org/10.2514/1.40932.

[10] Caruana, D., Mignosi, A., Corrège, M., Pourhiet, A. L., and Rodde, A., "Buffet and buffeting control in transonic flow," *Aerospace Science and Technology*, Vol. 9, 2005, pp. 605–616. http://doi.org/10.1016/j.ast.2004.12.005.

[11] Gao, C., Zhang, W., and Ye, Z., "Numerical study on closed-loop control of transonic buffet suppression by trailing edge flap," *Computers and Fluids*, Vol. 132, 2016, pp. 32–45. http://doi.org/10.2514/2.2071.

[12] Geoghegan, J., Giannelis, N., and Vio, G., "A Numerical Investigation of the Geometric Parametrisation of Shock Control Bumps for Transonic Shock Oscillation Control," *Fluids*, Vol. 12, 2020, pp. 1–29. http://doi.org/10.3390/fluids12083421.

[13] S. Gao, T. Y., Liu, P., and Qu, Q., "Flap upward deflection and rearward bump combination to alleviate transonic buffet of supercritical wing," *AIAA SciTech Forum 2018*, Kissimmee, FL, USA, 2018.

[14] Masini, L., Timme, S., and Pace, A. J., "Scale-Resolving Simulations of a Civil Aircraft Wing Transonic Shock-Buffet Experiment," *AIAA Journal*, Vol. 58, 2020, pp. 4322–4338. http://doi.org/10.2514/1.J059219.

[15] Ohmichi, Y., Ishida, T., and Hashimoto, A., "Modal Decomposition Analysis of Three-Dimensional Transonic Buffet Phenomenon on a Swept Wing," *AIAA Journal*, Vol. 56, 2018, pp. 3938–3950. http://doi.org/10.2514/1.J056855.

[16] Timme, S., "Global instability of wing shock-buffet onset," *Journal of Fluid Mechanics*, Vol. 885, 2020, p. A37. http://doi.org/10.1017/jfm.2019.1001.

[17] Lee, B., "Oscillatory shock motion caused by transonic shock boundary-layer interaction," *AIAA Journal*, Vol. 28, 1994, pp. 942–944. http://doi.org/10.2514/3.25144.

[18] Hartmann, A., Feldhusen, A., and Schröder, W., "On the interaction of shock waves and sound waves in transonic buffet," *Physics of Fluids*, Vol. 25, 2013, p. 026101. https://doi.org/10.1063/1.4791603.

[19] Feldhusen-Hoffmann, A., Statnikov, V., Klaas, M., and Schroder, W., "Investigation of shock–acoustic-wave interaction in transonic flow," *Experiments in Fluids*, Vol. 59, 2018, pp. 1–20. http://doi.org/10.1007/s00348-017-2466-z.

[20] Crouch, J., Gargaruk, A., and Magidov, D., "Predicting the onset of flow unsteadiness based on global instability," *Journal of Computational Physics*, Vol. 224, 2007, pp. 924–940. http://doi.org/10.1016/j.jcp.2006.10.035.

[21] Crouch, J., Gargaruk, A., Magidov, D., and Travin, A., "Origin of transonic buffet on aerofoils," *Journal of Fluid Mechanics*, Vol. 628, 2009, pp. 357–369. http://doi.org/10.1017/S0022112009006673.

[22] Crouch, J., Gargaruk, A., and Strelets, M., "Global instability in the onset of transonic-wing buffet," *Journal of Fluid Mechanics*, Vol. 881, 2019, pp. 3–22. http://doi.org/10.1017/jfm.2019.748.

[23] Babinsky, H., and Ogawa, H., "SBLI control for wings and inlets," *Shock Waves*, Vol. 18, 2008, pp. 89–96. http://doi.org/10.1007/s00193-008-0149-7.

[24] Pastrikakis, V., and Barakos, G., "Effect of active Gurney flaps on overall helicopter flight envelope," *The Aeronautical Journal*, Vol. 120, 2016, pp. 1230–1261. http://doi.org/10.1017/aer.2016.57.

[25] Steijl, R., Barakos, G., and Badcock, K., "A framework for CFD anal-ysis of helicopter rotors in hover and forward flight," *International Journal for Numerical Methods in Fluids*, Vol. 51, 2006, pp. 819–847. http://doi.org/10.1002/fld.1086.

[26] Steijl, R., and Barakos, G., "Sliding mesh algorithm for CFD analysis of helicopter rotor–fuselage aerodynamics," *International Journal for Numerical Methods in Fluids*, Vol. 58, 2008, pp. 527–549. http://doi.org/10.1002/fld.1757.

[27] Osher, S., and Chakravarthy, S., "Upwind schemes and boundary conditions with applications to Euler equations in general geometries," *Journal of Computational Physics*, Vol. 50, 1983, pp. 447–481. http://doi.org/10.1016/0021-9991(83)90106-7.

[28] van Leer, B., "Towards the ultimate conservative difference scheme. V. A second-order sequel to Godunov's method," *Journal of Computational Physics*, Vol. 32, 1979, pp. 101–136. http://doi.org/10.1016/0021-9991(79)90145-1.

[29] van Aldaba, G., van Leer, B., and Roberts, W., "A comparativestudy of computational methods in cosmic gas dynamics," *Astronomics and Astrophysics*, Vol. 108, 1982, pp. 76–84.

[30] Jameson, A., "Time-Dependent Calculations Using Multigrid, with Applications to Unsteady Flows past Airfoils and Wings," *AIAA 10th Computational Fluid Dynamics Conference*, 1991.

[31] Axelsson, O., *Iterative Solution Methods*, Cambridge University Press, 1994.

[32] Girimaji, S., and Abdol-Hamid, K., "Partially-averaged Navier Stokes Model for Turbulence: Implementation and Validation," *AIAA Aerospace Sciences Meeting and Exhibit*, Reno, NE, USA, 2005.

[33] Wilcox, D. C., "Formulation of the $k-\omega$ Turbulence Model Revisited," *AIAA Journal*, Vol. 46, 2008, pp. 2823–2838. http://doi.org/10.2514/1.36541.

[34] Lakshimpathy, S., Girimaji, S., and K.S., "Partially-averaged Navier Stokes method for turbulent flows: $k-\omega$ model implementation," *AIAA Aerospace Sciences Meeting and Exhibit*, Reno, NE, USA, 2006.

[35] Menter, F., "Two-equation eddy-viscosity turbulence models for engineering applications," *AIAA Journal*, Vol. 32, 1994, pp. 1598–1605. http://doi.org/10.2514/3.121495.

[36] Luo, D., Yan, C., and Wang, X., "Computational study of supersonic turbulent-separated flows using partially averaged Navier-stokes method," *Acta Astronautica*, Vol. 107, 2015, pp. 234–246. http://doi.org/10.1016/j.actaastro.2014.11.029.

[37] Woodgate, M. A., Pastrikakis, V. A., and Barakos, G. N., "Rotor Computations with Active Gurney Flaps," *Advances in Fluid-Structure Interaction*, edited by M. Braza, A. Bottaro, and M. Thompson, Springer International Publishing, 2016, pp. 133–166.

[38] Petrocchi, A., and Barakos, G., "Buffet boundary estimation using a harmonic balance method," *Aerospace Science and Technology*, Vol. 132, 2023, p. 108086. http://doi.org/10.1016/j.ast.2022.108086.

[39] Jacquin, L., Molton, P., Deck, S., Maury, B., and Soulevant, D., "An experimental study of shock oscillation over a transonic supercritical profile," *AIAA Aerospace Sciences Meeting and Exhibit*, Toronto, Ontario Canada, 2005.

[40] Jacquin, L., Molton, P., Deck, S., Maury, B., and Soulevant, D., "Experimental study of shock oscillation over a transonic supercritical profile," *AIAA Journal*, Vol. 47, 2009, pp. 1985–1994. http://doi.org/10.2514/1.30190.

[41] McDevitt, J., and A.F.Okuno, "Static and dynamic pressure measurements on a NACA 0012 airfoil in the Ames high Reynolds number facility," Tech. rep., National Aeronautics and Space Administration, 1985. NASA-TP-2485.

[42] Iovnovich, M., and Raveh, D. E., "Reynolds-Averaged Navier–Stokes Study of the Shock-Buffet Instability Mechanism," *AIAA Journal*, Vol. 50, 2012, pp. 880–890. http://doi.org/10.2514/1.J051329.

[43] Grossi, F., Braza, M., and Hoarau, Y., "Prediction of Transonic Buffet by Delayed Detached-Eddy Simulation," *AIAA Journal*, Vol. 52, 2014, pp. 2300–2312. http://doi.org/10.2514/1.J052873.